https://doi.org/10.5194/amt-2022-169
Preprint. Discussion started: 15 June 2022

Atmospheric Measurement Techniques Discussions

Improved spectral processing for a multi-mode pulse compression Ka/Ku-band cloud radar system

Han Ding[1,2], Haoran Li[2,3], Liping Liu[2]

[1]Collaborative Innovation Center on Forecast and Evaluation of Meteorological Disasters, Nanjing University of Information Science and Technology, Nanjing, China
[2]State Key Laboratory of Severe Weather, Chinese Academy of Meteorological Sciences, Beijing, China
[3]Institute for Atmospheric and Earth System Research/Physics, Faculty of Science, University of Helsinki, Helsinki, Finland

Correspondence to: Haoran Li (lihr@cma.gov.cn) and Liping Liu (liulp@cma.gov.cn)

Abstract. Cloud radars are widely used in observing clouds and precipitation. However, the raw data products of cloud radars are usually affected by multiple factors, which may lead to misinterpretation of cloud and precipitation processes. In this study, we present a Doppler-spectra-based data processing framework to improve the data quality of a multi-mode pulse-compressed Ka/Ku radar system. Firstly, non-meteorological clutter close to the ground was identified with enhanced Doppler spectral ratios between different observing modes. Then, the abnormal distribution of the probability density of the Doppler spectrum in presence of range sidelobe due to the implementation of the pulse compression technique was identified and used to separate sidelobe artifacts. Finally, the Doppler spectra observations from different modes were merged via the shift-then-average approach. The new radar moment products were generated based on the merged Doppler spectrum data. The presented spectral processing framework was applied to radar observations of a stratiform precipitation event, and the results show good performance of clutter/sidelobe suppression and spectral merging.

1. Introduction

Clouds and precipitation are important for the Earth's energy budget and the hydrological cycle. Over the past few decades, a great deal of effort has been made to understand the microphysics and dynamics of clouds and precipitation. As a remote sensing instrument, cloud radars operating in millimeter-wavelengths have shown their unique role in addressing the observational gaps in clouds and precipitation (Kollias et al., 2002; Stephens et al., 2002; Illingworth et al., 2007; Li and Moisseev, 2020). Compared with weather radars, shorter wavelengths of cloud radars allow for the

https://doi.org/10.5194/amt-2022-169
Preprint. Discussion started: 15 June 2022


Atmospheric Measurement Techniques Discussions

detection of small hydrometeors without the use of high-power transmitters and large antennas. Meanwhile, their compact size enables good portability, making them a powerful tool for observing clouds and weak precipitation (Kollias et al., 2007).

Most cloud radars work at the vertically pointing mode, and it is a common practice to use time-height plots to present the traditional radar data, such as equivalent reflectivity factor (Z_e), mean Doppler velocity (V), and spectrum width (σ). These data products are also known as the moments of radar Doppler spectrum which is the decomposition of the radar return as a function of Doppler velocities (Kollias et al., 2011a). Radar Doppler spectra observations have been used to retrieve the dynamics (Shupe et al., 2008; Li et al., 2021; e.g., Zhu et al., 2021) and microphysics (Luke and Kollias, 2013; Tridon et al., 2013; Verlinde et al., 2013; Kalesse et al., 2016; e.g., Kneifel et al., 2016) of clouds and precipitation. However, preprocessing of radar Doppler spectra observations can be challenging due to a list of issues:

1) The contamination of non-meteorological clutter. Narrow-beam-width antenna makes the cloud radars less susceptible to non-meteorological clutter in contrast to high-power long-wavelength radars (Kollias et al., 2007). To discriminate clutter echoes from clouds, some algorithms, e.g. based on the coherent characteristics of clouds (Kalapureddy et al., 2018), the Bayesian method (Hu et al., 2021), or polarimetric measurements (Martner and Moran, 2001), have been proposed. But such approaches fall short when meteorological signals are mixed with clutter. Alternatively, cloud/precipitation signals can be well reserved if the clutter removal is made in the radar Doppler spectrum (Luke et al., 2008; Moisseev and Chandrasekar, 2009; Williams et al., 2018; Williams et al., 2021). For example, for stationary ground clutter signals characterized by the Doppler velocity of around 0 m s^{-1}, an interpolation method can be performed to remove the clutter after identifying the narrow spectral peaks (Williams et al., 2018). Williams et al. (2021) have also used spectral linear depolarization ratio observations to identify asymmetric insect clutters. To the best of our knowledge, there is a lack of a non-polarimetric spectral approach to separate such non-stationary clutter signals.

2) The advance in solid-state amplifiers has led to the development of solid-state cloud radars. Solid-state transmitters are typically smaller, more reliable and more affordable than traditional vacuum tube type transmitters, but their output power is much lower than other types of tubes. To

https://doi.org/10.5194/amt-2022-169
Preprint. Discussion started: 15 June 2022

enhance the detection sensitivity, a wider pulse is used which on the other hand decreases the range resolution. The pulse compression techniques are widely employed to achieve high range resolutions, however, significant range sidelobe can be present around radar echoes. This may have a negligible impact on Z_e, but can severely affect the estimation of higher-order radar moments (Liu and Zheng, 2019). To remove the sidelobe artifacts introduced by the pulse compression, a simple threshold approach (Moran et al., 1998; Clothiaux et al., 1999) has been applied to radar moment products. To alleviate the range sidelobe contamination, the processors of Atmospheric Radiation Measurement (ARM) Millimeter Wavelength Cloud Radars (MMCRs) have been upgraded by reducing the number of code bits used in pulse-compressed modes (Moran et al., 2002). In China, pulse compression cloud radars are nationally deployed and sidelobe contamination is one of the major issues in radar data products. The threshold approach has been applied to the Doppler spectrum observations by Liu and Zheng (2019). However, the best power threshold always needs to be adjusted according to the received signal, and sometimes several rounds of processing are required.

3) Multiple operating modes have been employed to address the trade-off among the sensitivity, spatial and temporal resolution, Nyquist velocity, and maximum unambiguous range. For modes with pulse compression techniques, the emitting of long pulses leads to an increase in radar blind range, limiting the capability of mapping the vertical distributions of clouds. However, the blind zones and sensitivities of different observing modes are different, leaving complicated data processing procedures in radar applications.

In this study, we present an improved data processing framework to tackle the above-mentioned issues. Section 2 describes the radars used in this study, followed by clutter and sidelobe artifact removal algorithms in Sect. 3. The merging of Doppler spectra observations at different modes is given in Sect. 4. The new data processing framework was applied to radar observations of a stratiform precipitation event and the results are analyzed in Sect. 5. Conclusions are presented in Sect. 6.

2. Data

The vertically pointing Ka/Ku dual-frequency radar used in this paper has been operating at the Longmen Observation Station (114.27°E, 23.79°N) in southeastern China since 2019. The

https://doi.org/10.5194/amt-2022-169
Preprint. Discussion started: 15 June 2022

Atmospheric Measurement Techniques Discussions

operating parameters of four observation modes are shown in Table 1. Both radars are implemented with solid-state transmitters and pulse compression techniques. The maximum detection range is 15 km and the range resolution of 30 m. The antenna beamwidth is 0.9° for the Ku-band radar and 0.35° for the Ka-band. Both radars operate with four modes: boundary layer mode (mode 1), cirrus mode (mode 2), precipitation mode (mode 3), and middle-level mode (mode 4). These four modes are characterized by different pulse compression ratios, numbers of coherent integration as well as incoherent integration. The boundary layer mode aims to detect low-level clouds and a narrower pulse waveform as well as a larger number of coherent integrations is used to improve the detection ability. The cirrus mode uses the pulse compression technique to improve the sensitivity to detect clouds with weaker radar echoes at higher latitudes. The middle-level mode also uses pulse compression techniques but less coherent integration times. The precipitation mode is characterized by a larger unambiguous range and velocity for rainfall observations. There are four different modes routinely cycled in operations and each mode takes 7 s to finish the observation. The radar Doppler spectra are computed using a 256-point fast Fourier transform (FFT). The resolutions of spectral velocity at all modes are interpolated into 0.072 m s^{-1} (Ka-band radar) and 0.09 m s^{-1} (Ku-band radar). The spectral noise floor is determined using the Hilderbrand-Sekhon method (Hildebrand and Sekhon, 1974). It should be noted that due to the use of long pulses in mode 2 and mode 4 for both radars, the heights below 2 km and 1 km are blind zones, respectively. In addition, the Nyquist velocity of the Ka-band radar at mode 1 is 4.6 m s^{-1}, and the observed Doppler spectrum easily gets aliased therefore the Ka-band radar observations at mode 1 were not used.

Table 1. Operating parameters for the Ka/Ku-band cloud radar system deployed at Longmen observation station in southeastern China.

Parameters	Mode 1	Mode 2	Mode 3	Mode 4
Pulse width (μs)	0.2	12	0.2	6
Range resolution (m)	30	30	30	30
Nyquist velocity of Ka-band (m s^{-1})	4.63	9.27	18.54	18.54
Nyquist velocity of Ku-band (m s^{-1})	11.48	22.97	45.95	45.95
Spectral velocity resolution of Ka-band (m s^{-1})	0.036	0.072	0.145	0.145
Spectral velocity resolution of Ku-band (m s^{-1})	0.09	0.18	0.36	0.36
Number of coherent integrations	4	2	1	1
Number of incoherent integrations	16	32	64	64
Number of points in FFT	256	256	256	256

https://doi.org/10.5194/amt-2022-169
Preprint. Discussion started: 15 June 2022


Atmospheric Measurement Techniques Discussions

3. Clutter and range sidelobe mitigation

Clutter contamination is a long-standing issue in scanning and vertically pointing radar observations. Both ground clutter and insect clutter obscure the boundary layer returns, affecting the high-order moments estimated from Doppler spectra observations (Sato and Woodman, 1982). In addition, the implementation of pulse compression techniques in modes 2 and 4 usually results in significant range sidelobe around the melting layer, which does not significantly affect Z_e and V estimates, but can severely degrade the estimation of spectrum width. In this section, Ku-band radar observations are used to demonstrate the spectral processing procedure for mitigating the clutter contamination and range sidelobe.

3.1 Clutter mitigation

The stationary ground clutter is usually manifested as a narrow-symmetric peak around 0 m s^{-1} (Williams et al., 2018). A commonly used approach for mitigating ground clutter signals is the interpolation of adjacent spectral powers after removing the spectral peak around 0 m s^{-1}. Williams et al. (2018) claimed that this method is also suitable for the identification and removal of insect clutters since the insect targets also produce narrow peaks in Doppler spectra observations. We have tried to apply this approach to our radar data, but the performance is not as good as that for the Ka-band zenith pointing radar (KAZR) deployed at Oliktok Point, Alaska. Figure 1a shows an example of the Ku-band Doppler spectrum with clutter signals present at around 0 m s^{-1}. The clutter signals do not always present a sharp narrow peak as shown in Fig. 3 in Williams et al. (2018), and this approach does not apply to our observations. We have also found that such clutter signals appear more frequently and significantly in Ku-band radar observations than in the Ka-band. Compared with coherent meteorological signals, such clutter signals vary drastically among different observing modes (Fig. 1a). This is plausibly attributed to different compression ratios at the four modes. The cause of such clutter signals is unclear yet and we hesitate to classify them to insects (Williams et al., (2018), since the spectral powers at different modes deviate from each other significantly.

https://doi.org/10.5194/amt-2022-169
Preprint. Discussion started: 15 June 2022

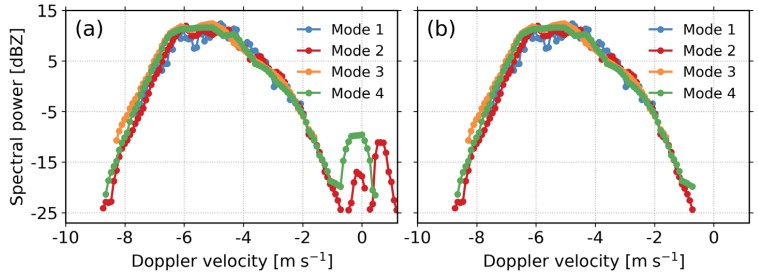

Figure 1. (a) Noise-removed Ku-band Doppler power spectrum on 6 June 2020 at 22:52:08 LST at the range of 2.34 km. (b) Same as (a) but decluttered with our clutter mitigation algorithm.

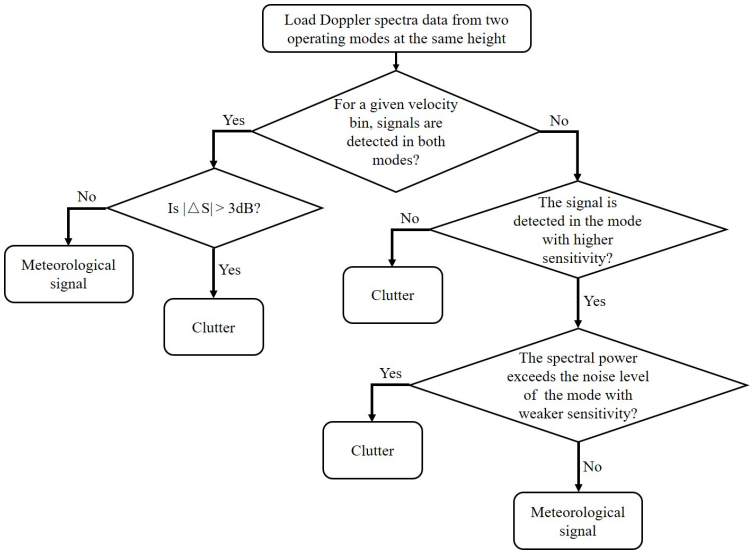

Figure 2. Flow chart of the proposed clutter identification and mitigation method

As shown in Fig. 2, we have developed an algorithm to identify and remove clutter signals. The algorithm is mainly based on the non-coherent nature of clutters which produces significant spectral power ratio (ΔS) between observations from different modes. The selection of $|\Delta S| = 3$ dB is a compromise between the radars' observational uncertainty and the spectral ratio between different observing modes. As shown in Fig. 1b, clutter signals have been successfully removed while the meteorological signals are marginally affected.

Figure 3 compares the Doppler spectrum observations before and after applying the declutter algorithm. As shown in Fig. 3a_1 and c_1, the clutter signals appear below 2 km at modes 1 and 3. For modes 2 and 4, the impact of clutter can be up to 3 km (Fig. 3b_1 and d_1). After imposing the declutter

https://doi.org/10.5194/amt-2022-169
Preprint. Discussion started: 15 June 2022

Atmospheric Measurement Techniques Discussions

algorithm, no significant clutter signals can be detected (Fig. 3a_2, b_2, c_2, and d_2).

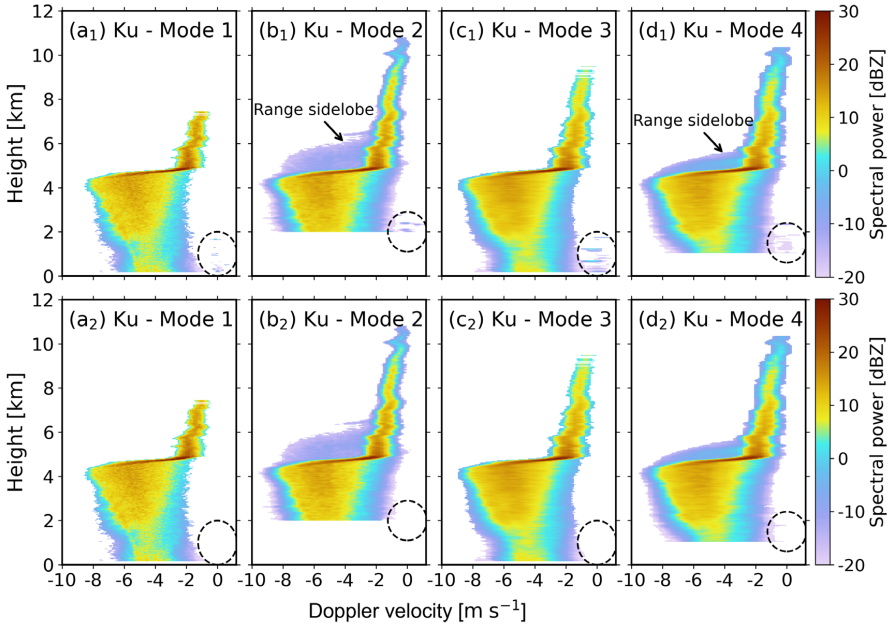

Figure 3. Top: noise-removed Ku-band Doppler power spectra on 6 June 2020 at 22:52:08 LST recorded at (a_1) mode 1, (b_1) mode 2, (c_1) mode 3, (d_1) mode 4. Bottom: decluttered observations. The dashed circles mark the clutter signals. Note that the heights below 2 km and 1 km are blind zones for modes 2 and 4, respectively.

3.2 Range sidelobe artifacts

The utilization of pulse compression usually leads to range sidelobe artifacts (Fig 3. b_1 and d_1) around strong radar echoes, which can severely affect the estimates of high-order radar moments. Moran has proposed an approach that distinguishes the range sidelobe artifacts from reflectivity data using non-range-corrected return power through the power transfer function (Moran et al., 1998; Clothiaux et al., 1999). By reducing the number of code bits used in pulse compression modes, the ARM MMCRs' upgraded processor is capable of suppressing the range sidelobe effects (Moran et al., 2002). However, mitigating range sidelobe artifacts is still challenging for multi-mode pulsed-compression cloud radars in China. Liu and Zheng (2019) have applied the method proposed by Moran et al. (1998) to radar Doppler spectrum data to remove the range sidelobe artifacts. However, the performance of this approach depends on a given threshold, which needs to be adjusted for different scenarios. In addition, we found that this method seems applicable to the Ka-band radar,

https://doi.org/10.5194/amt-2022-169
Preprint. Discussion started: 15 June 2022

Atmospheric Measurement Techniques Discussions

but the artifact removal performance of the Ku-band radar is far inferior to that of the Ka-band.

As shown in Fig. 3b$_1$ and d$_1$, the range sidelobe associated with the strong radar echoes of the melting particles is located above the melting layer. Compared with radar Doppler spectrum observations without the sidelobe contamination (see for example (Li and Moisseev, 2020)), the sidelobe caused by the pulse compression drags a long tail in the relatively large velocity bins and the characteristics of the two tails are slightly different (Fig. 3b$_1$ and d$_1$). The artifacts in mode 2 accumulate to higher altitudes but are weaker in spectral power (Fig. 3b$_1$), while mode 4 accumulates to lower altitudes and with a larger magnitude of power (Fig. 3d$_1$).

An interesting feature of the tail caused by the range sidelobe is that its spectral power is much flatter than cloud and precipitation signals. Figure 4a shows the probability density functions (PDFs) of received spectral power from 2 km and 7 km. The PDFs at different heights are detectably different. For Doppler spectra without the sidelobe contamination, PDFs are relatively uniform. In contrast, for the sidelobe-contaminated Doppler spectrum, the peak of the PDFs appears close to the noise level and is mostly below 15 dB above the noise level. A closer look into the radar Doppler spectra at 5.01 km (Fig. 5a) shows that the strong PDF peak in Fig. 4a is explained by the relatively flat range sidelobe signals. Here, we introduce a parameter spectral power threshold (S_{thresh}) to distinguish the range sidelobe from meteorological signals. Figure 6 shows the flowchart for the identification and removal of the range sidelobe artifacts. The procedures are briefly summarized as follows,

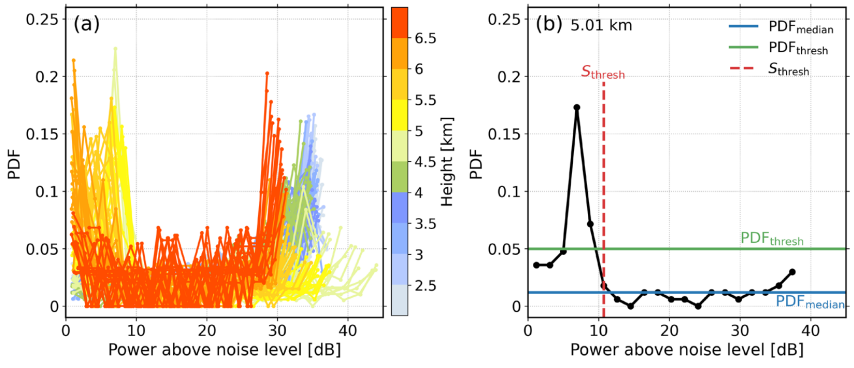

Figure 4. (a): PDFs of Doppler spectra from 2 km to 7 km at mode 2; (b): PDF of Doppler spectrum recorded at 5.01 km.

https://doi.org/10.5194/amt-2022-169
Preprint. Discussion started: 15 June 2022

Atmospheric Measurement Techniques Discussions

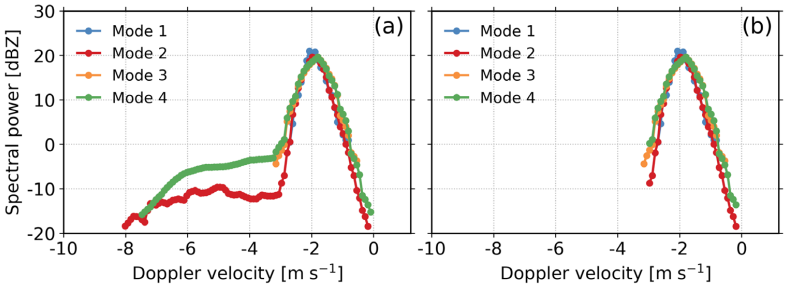

Figure 5. Ku-band Doppler power spectra recorded at different modes at 5.01 km on 6 June 2020 at 22:52:08 LST. (a) Noise-removed Doppler spectrum; (b) the same as (a) but after the removal of range sidelobe.

1) Sort the spectral power values above noise level in an ascending order to get a PDF curve of each Doppler spectrum;

2) Calculate the median and standard deviation (SD) of the PDFs, set $PDF_{thresh} = PDF_{median} + PDF_{SD}$;

3) Below half of the peak power above the noise level of the Doppler spectrum, find the power bins' probability density just exceeds the PDF_{thresh}, and the corresponding spectral power is set as S_{thresh};

4) If the spectrum power with the Doppler velocity larger than the mean Doppler velocity is below the S_{thresh}, then it is flagged as sidelobe.

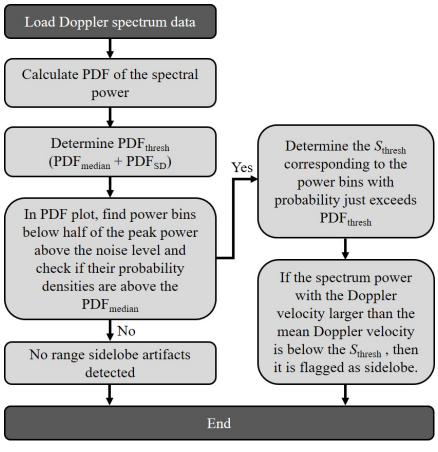

Figure 6. Flowchart of range sidelobe artifacts processing

https://doi.org/10.5194/amt-2022-169
Preprint. Discussion started: 15 June 2022

Atmospheric Measurement Techniques Discussions

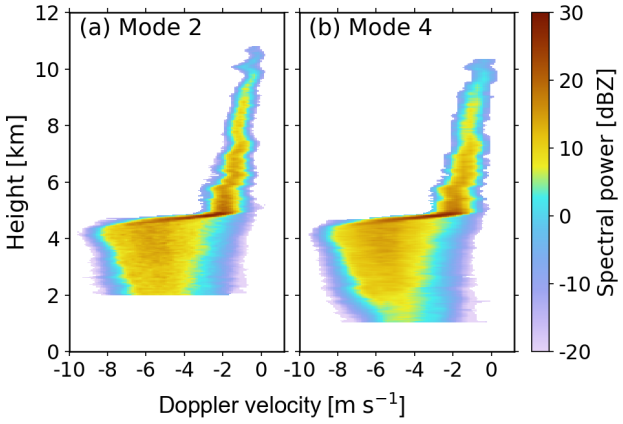

Figure 7. Doppler power spectra after removing range sidelobe at modes 2 and 4 on 6 June 2020 at 22:52:08 LST. The Doppler spectra observations before the sidelobe removal are shown in Fig. 3b$_1$ and d$_1$.

As shown in Fig. 5b, the range sidelobe artifacts in modes 2 and 4 have been well removed. We have applied this algorithm to the vertical profiles of Doppler spectra observations at modes 2 and 4 (Fig. 3b$_1$ and 3d$_1$). As shown in Fig. 7a and 7b, the sidelobe artifacts have been well removed at modes 2 and 4.

4. Mode merging

For multi-mode cloud radars, it is cumbersome to interpretate the radar observations recorded at four modes in operational applications. Moreover, the air motion variability and the velocity bin-to-bin spectrum power fluctuations can lead to noisy estimates of high-order spectrum moments. Therefore, we have merged radar observations from different observing modes.

4.1 Merging of Doppler spectra recorded at different modes

Before the merging procedure, it is necessary to check the consistency of radar data at four modes. Particularly, coherent integrations were made to modes 1 and 2 (Tab.1) to improve the signal-to-noise ratio. But this step may result in the decrease of spectral power with large Doppler velocities (Liu et al., 2017; Liu and Zheng, 2019). This effect leads to the underestimation of V, which is critical in the merging process, and Z_e. Here, we evaluate this impact by comparing Z_e and V estimates at different modes. We define the differences of Z_e and V between different modes as ΔZ and ΔV, respectively, and radar observations at mode 3 (no pulse compression and only one round coherent integration were performed) were used as a reference. To compare the impact of coherence

https://doi.org/10.5194/amt-2022-169
Preprint. Discussion started: 15 June 2022

Atmospheric Measurement Techniques Discussions

integration under various precipitation intensities, radar observations were grouped into $Z_e > 20$ dBZ and $Z_e < 10$ dBZ. Note that the Ku-band wet radome attenuation has been corrected with a collocated C-band radar (Cui et al., 2020).

In light precipitation ($Z_e < 10$ dBZ, Fig. 8a_1, 8b_1, and 8c_1), radar observations at these four modes agree with each other rather well. For precipitation cases with $Z_e > 20$ dBZ, good agreement between modes 3 and 4 can also be found (Fig. 8c_2), which is expected since the coherent integration number is one at both modes. The agreement between modes 2 and 3 seems also good (Fig. 8b_2), despite two rounds of coherent integration were made to mode 2. In Fig. 8a_1, significant biases of ΔZ and ΔV can be identified, and ΔV increases with ΔZ. This is attributed to the underestimation of spectrum powers at high Doppler velocities during the longtime coherent integration (4 rounds). Given the results above, Ku-band Doppler spectra observations at mode 1 were discarded.

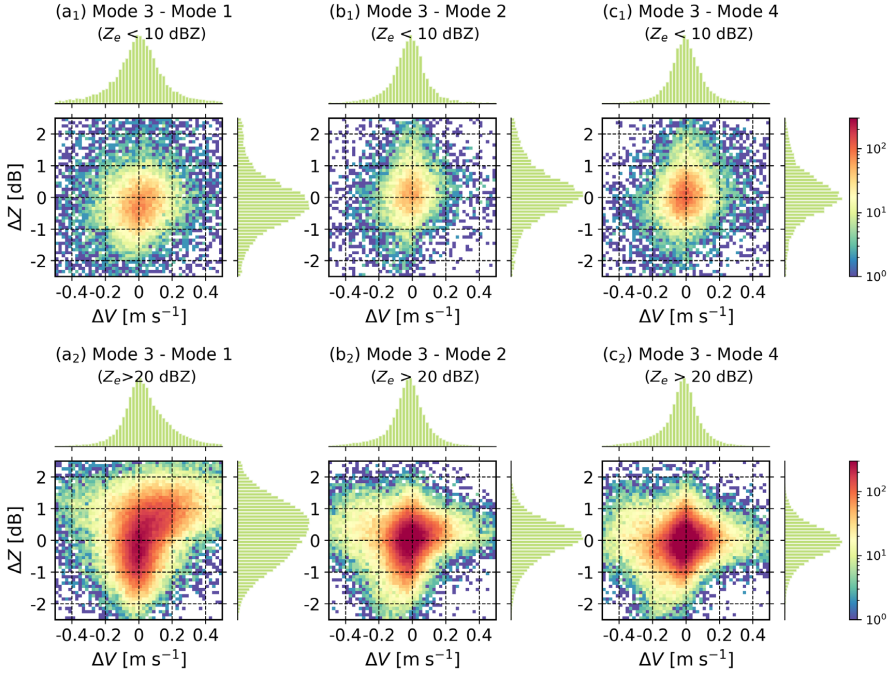

Figure 8. Statistics of ΔZ and ΔV for the Ku-band radar. Top: precipitation cases with $Z_e > 20$ dBZ; Bottom: precipitation cases with $Z_e < 10$ dBZ.

4.2 Shift-then-average spectra

To maximize the detection advantages of each mode, and to obtain high-quality and easy-to-

https://doi.org/10.5194/amt-2022-169
Preprint. Discussion started: 15 June 2022

Atmospheric Measurement Techniques Discussions

use radar datasets, Doppler spectra observations from the modes 2, 3, and 4 were merged as follows (Giangrande et al., 2001; Luke and Kollias, 2013; Williams et al., 2018),

1) Velocity shift: set the mean of the mean Doppler velocity at each mode as the reference velocity, and then shift the Doppler spectrum at each mode to match the mean Doppler velocities at all modes;

2) Spectral power average: average the spectral powers observed at all modes in each observation round.

We have applied this algorithm to Ku-band radar Doppler spectra observations, and an example is presented in Fig. 9. The merged Doppler spectrum is significantly less uncertain thanks to the averaging process. It should be noted that the drawback of the mode merging is that the time resolution changes from 7 s to 28 s.

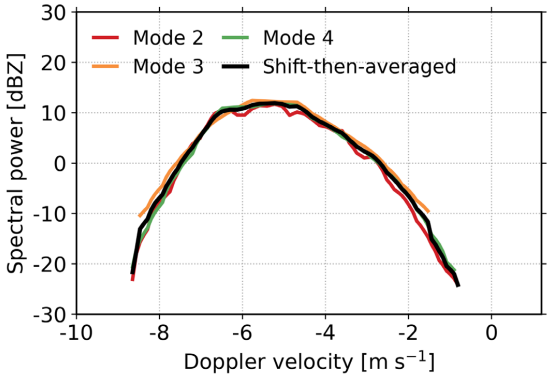

Figure 9. Ku-band Doppler velocity spectra from modes 2, 3 and 4 recorded on 6 June 2020 at 22:52:08 LST at 2.34 km. The merged Doppler spectrum is derived from the Doppler spectra recorded at modes 2, 3, and 4 after shifting and averaging.

High-order moments of the Doppler spectrum are representative of the key microphysical processes in clouds and precipitation (Luke and Kollias, 2013; Maahn and Löhnert, 2017; Li et al., 2021). The second, third, and fourth moments of the radar Doppler spectrum are spectrum width, skewness, and kurtosis respectively. Figure 10 compares these high-order moments estimated from the Ku-band radar Doppler spectra at modes 2, 3, 4, and the merged data. The sidelobe impacts on spectrum width, skewness, and kurtosis are significant between 5 and 7 km at modes 2 and 4 (Fig. 10 a, b, c). In rain, the estimates of high-order moments at modes 2, 3, and 4 agree rather well with

https://doi.org/10.5194/amt-2022-169
Preprint. Discussion started: 15 June 2022

Atmospheric Measurement Techniques Discussions

each other. In snow, the spectrum width at mode 2 is systematically smaller than those at other modes (Fig. 10a). This may be explained by the finer spectral velocity resolution at mode 2 (Tab. 1). In addition, as the radar echo approaches to the noise level, underestimation of kurtosis becomes more significant (mode 3 in Fig. 10c). The results for the Ka-band radar are shown in Fig. 11. Although the agreement among different modes is better than that at Ku-band thanks to higher spectral velocity resolution and less uncertainties for the Ka-band radar, while the bias of kurtosis in snow at mode 3 (Fig. 11c) is more contrasting. These findings indicate that the uncertainties of estimated radar moments as introduced by different observing modes should be taken into account in snow retrievals (Maahn and Löhnert, 2017).

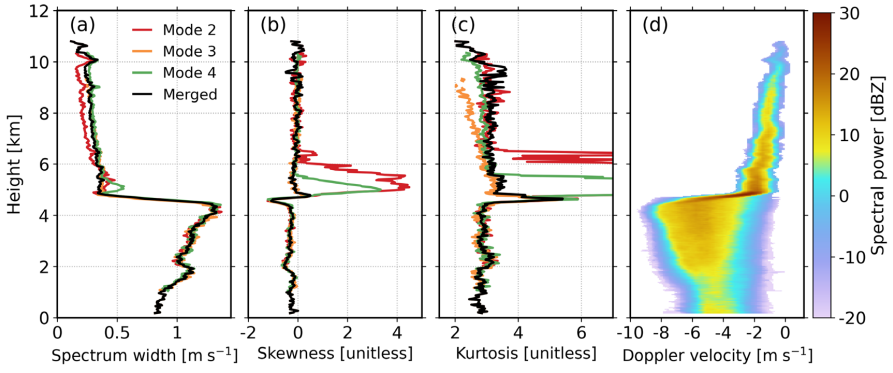

Figure 10. (a) Spectrum width, (b) skewness and (c) kurtosis estimated from Ku-band radar Doppler spectra recorded at mode 2, 3, 4 and the merged data; (d) the profile of merged Doppler velocity spectra.

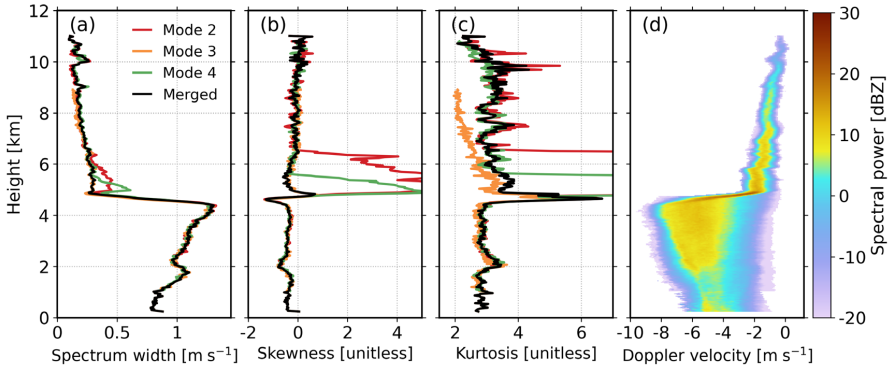

Figure 11. Same as Fig. 10 but for Ka-band radar.

https://doi.org/10.5194/amt-2022-169
Preprint. Discussion started: 15 June 2022


Atmospheric Measurement Techniques Discussions

5. Case study

A stratiform precipitation system moved over the Longmen station on 6 June 2020. To evaluate the performance of the presented framework, the merged radar products were compared with raw data products at mode 3. The time-height cross-section plots of Ku- and Ka-band radar observations are shown in Fig. 12 and 13, respectively. The cloud top height is about 14 km (Fig. 12a$_1$), while it is much lower at mode 3 (9 ~ 10 km) which is attributed to the lower sensitivity at this mode. At Ka-band, due to the increased attenuation from rain, melting layer, and the wet radome (Li and Moisseev, 2019), the observed cloud top descends to around 7 km during the most intensive precipitation period (around 22:00 LST, Fig. 13a$_2$).

Skewness and kurtosis are indicative of the degree of asymmetry and peakness of the spectrum, respectively. Skewness has been used as an early qualitative predictor of drizzle onset in clouds and locating supercooled liquid water since it is very sensitive to drizzle generation (Luke et al., 2010; Kollias et al., 2011a; Kollias et al., 2011b). The higher-order radar moments have been less frequently used for studying the melting layer. It appears that skewness presents a "decrease-increase-decrease" feature, while kurtosis is characterized by a distinct enhancement. These observations of skewness and kurtosis in the melting layer are interesting, and how these changes are linked to the change of cloud/precipitation microphysics warrants future studies.

https://doi.org/10.5194/amt-2022-169
Preprint. Discussion started: 15 June 2022

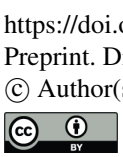

Atmospheric Measurement Techniques Discussions

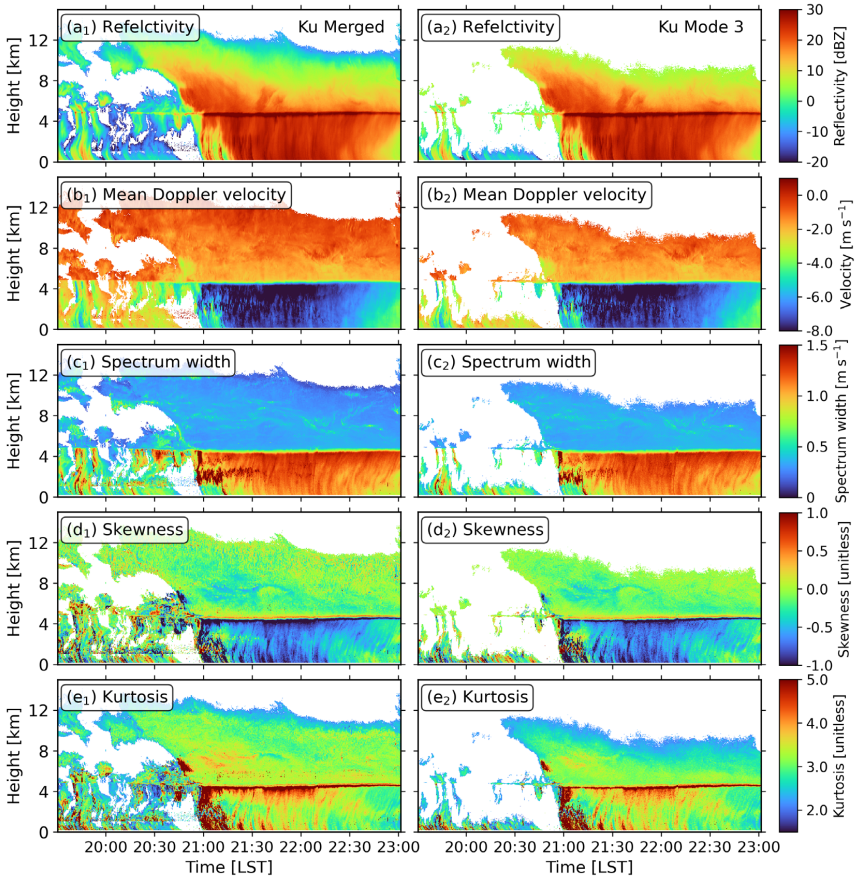

Fig 12. Time-height cross-section plots of Ku-band Doppler spectra moments from 19:30:19 to 23:01:26, the left column is estimated from the merged Doppler spectra and the right column is from the data recorded at mode 3. From top to bottom: (a) reflectivity; (b) mean Doppler velocity; (c) spectrum width; (d) skewness; (e) kurtosis.

https://doi.org/10.5194/amt-2022-169
Preprint. Discussion started: 15 June 2022

Atmospheric Measurement Techniques Discussions

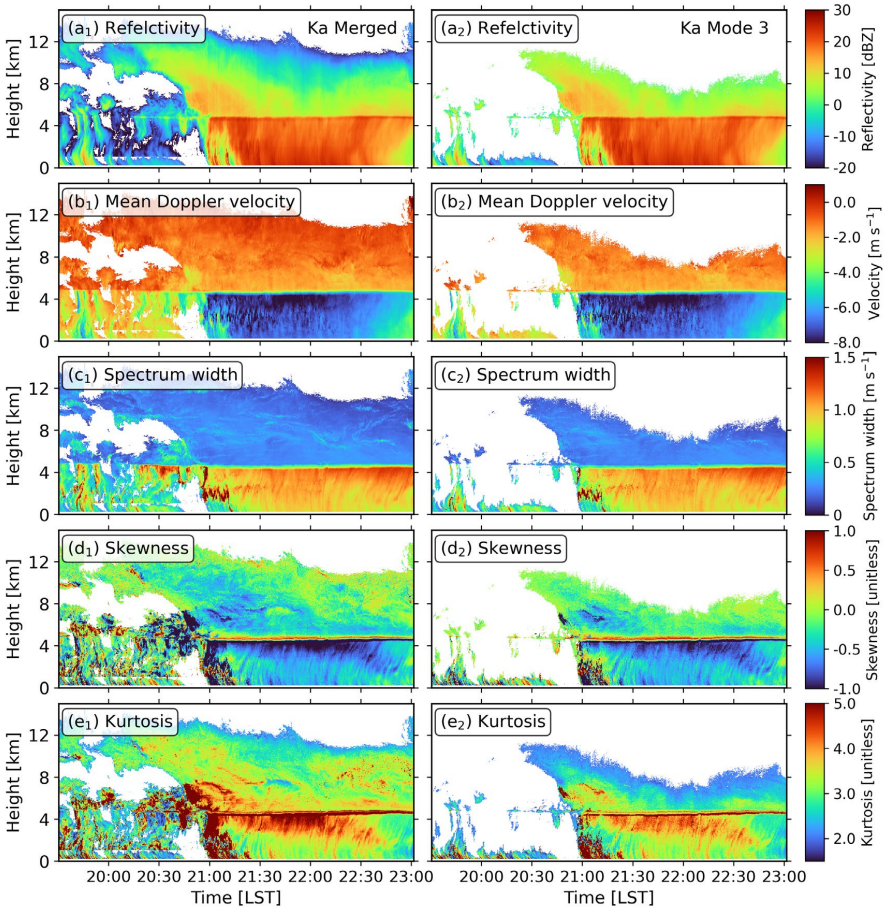

Figure 13. same as Fig. 12 but in Ka-band.

305

6. Summary

In this study, a framework for processing the Doppler spectra observations of a multi-mode pulse compression Ka/Ku cloud radar system is presented. We first proposed an approach to identify and remove the clutter signals in the Doppler spectrum based on spectral power ratios between 310 different operating modes. Then, we developed a new algorithm to remove the range sidelobe around the melting layer at the modes implementing the pulse compression technique. The radar observations from different modes were then merged using the shift-then-average method. The presented spectral processing framework was applied to radar observations of a stratiform precipitation event, and the results show good performance of clutter/sidelobe suppression and

https://doi.org/10.5194/amt-2022-169
Preprint. Discussion started: 15 June 2022

spectral merging. The multi-year radar observations recorded at the Longmen station will be processed with the present framework for elucidating the dynamics and microphysics of clouds and precipitation in southern China.

Author contributions. HL and LL conceptualized this study; HD performed the investigation and wrote the draft. All authors contributed to reviewing and editing of the manuscript.

Competing interests. The authors declare that they have no conflict of interest.

Financial support. This research has been supported by the National Natural Science Foundation of China (grant no. 41875036, U2142210).

References

Clothiaux, E. E., Moran, K. P., Martner, B. E., Ackerman, T. P., Mace, G. G., Uttal, T., Mather, J. H., Widener, K. B., Miller, M. A., and Rodriguez, D. J.: The Atmospheric Radiation Measurement Program Cloud Radars: Operational Modes, J. Atmos. Ocean. Tech., 16, 819-827, 10.1175/1520-0426(1999)016<0819:Tarmpc>2.0.Co;2, 1999.

Cui, Y., Ruan, Z., Wei, M., Li, F., and Ge, R.: Vertical structure and dynamical properties during snow events in middle latitudes of China from observations by the C-band vertically pointing radar, J. Meteorol. Soc. Jpn. Ser. II, 2020.

Giangrande, S. E., Babb, D. M., and Verlinde, J.: Processing Millimeter Wave Profiler Radar Spectra, J. Atmos. Ocean. Tech., 18, 1577-1583, 10.1175/1520-0426(2001)018<1577:Pmwprs>2.0.Co;2, 2001.

Hildebrand, P. H. and Sekhon, R.: Objective determination of the noise level in Doppler spectra, J. Appl. Meteorol., 13, 808-811, 1974.

Hu, X., Ge, J., Du, J., Li, Q., Huang, J., and Fu, Q.: A robust low-level cloud and clutter discrimination method for ground-based millimeter-wavelength cloud radar, Atmos. Meas. Tech., 14, 1743-1759, 10.5194/amt-14-1743-2021, 2021.

Illingworth, A. J., Hogan, R. J., O'Connor, E. J., Bouniol, D., Brooks, M. E., Delanoé, J., Donovan, D. P., Eastment, J. D., Gaussiat, N., Goddard, J. W. F., Haeffelin, M., Baltink, H. K., Krasnov, O. A., Pelon, J., Piriou, J.-M., Protat, A., Russchenberg, H. W. J., Seifert, A., Tompkins, A. M., van Zadelhoff, G.-J., Vinit, F., Willén, U., Wilson, D. R., and Wrench, C. L.: Cloudnet: Continuous Evaluation of Cloud Profiles in Seven Operational Models Using Ground-Based Observations, B. Am. Meteorol. Soc., 88, 883-898, 10.1175/bams-88-6-883, 2007.

Kalapureddy, M. C. R., Sukanya, P., Das, S. K., Deshpande, S. M., Pandithurai, G., Pazamany, A. L., Ambuj K, J., Chakravarty, K., Kalekar, P., and Devisetty, H. K.: A simple biota removal algorithm for 35 GHz cloud radar measurements, Atmos. Meas. Tech., 11, 1417-1436, 2018.

Kalesse, H., Szyrmer, W., Kneifel, S., Kollias, P., and Luke, E.: Fingerprints of a riming event on cloud

https://doi.org/10.5194/amt-2022-169
Preprint. Discussion started: 15 June 2022

radar Doppler spectra: observations and modeling, Atmos. Chem. Phys., 16, 2997-3012, 10.5194/acp-16-2997-2016, 2016.

Kneifel, S., Kollias, P., Battaglia, A., Leinonen, J., Maahn, M., Kalesse, H., and Tridon, F.: First observations of triple-frequency radar Doppler spectra in snowfall: Interpretation and applications, Geophys. Res. Lett., 43, 2225-2233, 2016.

Kollias, P., Albrecht, B. A., and Jr., F. M.: Why Mie?, B. Am. Meteorol. Soc., 83, 1471-1484, 10.1175/bams-83-10-1471, 2002.

Kollias, P., Rémillard, J., Luke, E., and Szyrmer, W.: Cloud radar Doppler spectra in drizzling stratiform clouds: 1. Forward modeling and remote sensing applications, J. Geophys. Res.-Atmos., 116, 2011a.

Kollias, P., Szyrmer, W., Rémillard, J., and Luke, E.: Cloud radar Doppler spectra in drizzling stratiform clouds: 2. Observations and microphysical modeling of drizzle evolution, J. Geophys. Res.-Atmos., 116, https://doi.org/10.1029/2010JD015238, 2011b.

Kollias, P., Clothiaux, E. E., Miller, M. A., Albrecht, B. A., Stephens, G. L., and Ackerman, T. P.: Millimeter-Wavelength Radars: New Frontier in Atmospheric Cloud and Precipitation Research, B. Am. Meteorol. Soc., 88, 1608-1624, 10.1175/bams-88-10-1608, 2007.

Li, H. and Moisseev, D.: Melting Layer Attenuation at Ka- and W-Bands as Derived From Multifrequency Radar Doppler Spectra Observations, J. Geophys. Res.-Atmos., 124, 9520-9533, https://doi.org/10.1029/2019JD030316, 2019.

Li, H. and Moisseev, D.: Two Layers of Melting Ice Particles Within a Single Radar Bright Band: Interpretation and Implications, Geophys. Res. Lett., 47, e2020GL087499, https://doi.org/10.1029/2020GL087499, 2020.

Li, H., Korolev, A., and Moisseev, D.: Supercooled liquid water and secondary ice production in Kelvin–Helmholtz instability as revealed by radar Doppler spectra observations, Atmos. Chem. Phys., 21, 13593-13608, 10.5194/acp-21-13593-2021, 2021.

Liu, L. and Zheng, J.: Algorithms for Doppler Spectral Density Data Quality Control and Merging for the Ka-Band Solid-State Transmitter Cloud Radar, Remote Sens., 11, 209, 2019.

Liu, L., Zheng, J., and Wu, J.: A Ka-band solid-state transmitter cloud radar and data merging algorithm for its measurements, Adv. Atmos. Sci., 34, 545-558, 10.1007/s00376-016-6044-8, 2017.

Luke, E. P. and Kollias, P.: Separating cloud and drizzle radar moments during precipitation onset using Doppler spectra, J. Atmos. Ocean. Tech., 30, 1656-1671, 2013.

Luke, E. P., Kollias, P., and Shupe, M. D.: Detection of supercooled liquid in mixed-phase clouds using radar Doppler spectra, J. Geophys. Res.-Atmos., 115, https://doi.org/10.1029/2009JD012884, 2010.

Luke, E. P., Kollias, P., Johnson, K. L., and Clothiaux, E. E.: A Technique for the Automatic Detection of Insect Clutter in Cloud Radar Returns, J. Atmos. Ocean. Tech., 25, 1498-1513, 10.1175/2007jtecha953.1, 2008.

Maahn, M. and Löhnert, U.: Potential of Higher-Order Moments and Slopes of the Radar Doppler Spectrum for Retrieving Microphysical and Kinematic Properties of Arctic Ice Clouds, J. Appl. Meteorol. Clim., 56, 263-282, 10.1175/jamc-d-16-0020.1, 2017.

Martner, B. E. and Moran, K. P.: Using cloud radar polarization measurements to evaluate stratus cloud and insect echoes, J. Geophys. Res.-Atmos., 106, 4891-4897, https://doi.org/10.1029/2000JD900623, 2001.

Moisseev, D. N. and Chandrasekar, V.: Polarimetric Spectral Filter for Adaptive Clutter and Noise Suppression, J. Atmos. Ocean. Tech., 26, 215-228, 10.1175/2008jtecha1119.1, 2009.

Moran, K., Martner, B., Clark, K., and Chanders, C.: Forthcoming Upgrades to the ARM MMCRs:

https://doi.org/10.5194/amt-2022-169
Preprint. Discussion started: 15 June 2022

Improved Radar Processor and Dual-Polarization, 2002.

Moran, K. P., Martner, B. E., Post, M. J., Kropfli, R. A., Welsh, D. C., and Widener, K. B.: An Unattended Cloud-Profiling Radar for Use in Climate Research, B. Am. Meteorol. Soc., 79, 443-456, 10.1175/1520-0477(1998)079<0443:Aucprf>2.0.Co;2, 1998.

Sato, T. and Woodman, R. F.: Spectral parameter estimation of CAT radar echoes in the presence of fading clutter, Radio. Sci., 17, 817-826, https://doi.org/10.1029/RS017i004p00817, 1982.

Shupe, M. D., Kollias, P., Persson, P. O. G., and McFarquhar, G. M.: Vertical Motions in Arctic Mixed-Phase Stratiform Clouds, J. Atmos. Sci., 65, 1304-1322, 10.1175/2007jas2479.1, 2008.

Stephens, G. L., Vane, D. G., Boain, R. J., Mace, G. G., Sassen, K., Wang, Z., Illingworth, A. J., O'connor, E. J., Rossow, W. B., Durden, S. L., Miller, S. D., Austin, R. T., Benedetti, A., and Mitrescu, C.: THE CLOUDSAT MISSION AND THE A-TRAIN: A New Dimension of Space-Based Observations of Clouds and Precipitation, B. Am. Meteorol. Soc., 83, 1771-1790, 10.1175/bams-83-12-1771, 2002.

Tridon, F., Battaglia, A., and Kollias, P.: Disentangling Mie and attenuation effects in rain using a Ka-W dual-wavelength Doppler spectral ratio technique, Geophys. Res. Lett., 40, 5548-5552, https://doi.org/10.1002/2013GL057454, 2013.

Verlinde, J., Rambukkange, M. P., Clothiaux, E. E., McFarquhar, G. M., and Eloranta, E. W.: Arctic multilayered, mixed-phase cloud processes revealed in millimeter-wave cloud radar Doppler spectra, J. Geophys. Res.-Atmos., 118, 13,199-113,213, https://doi.org/10.1002/2013JD020183, 2013.

Williams, C. R., Maahn, M., Hardin, J. C., and de Boer, G.: Clutter mitigation, multiple peaks, and high-order spectral moments in 35 GHz vertically pointing radar velocity spectra, Atmos. Meas. Tech., 11, 4963-4980, 10.5194/amt-11-4963-2018, 2018.

Williams, C. R., Johnson, K. L., Giangrande, S. E., Hardin, J. C., Öktem, R., and Romps, D. M.: Identifying insects, clouds, and precipitation using vertically pointing polarimetric radar Doppler velocity spectra, Atmos. Meas. Tech., 14, 4425-4444, 10.5194/amt-14-4425-2021, 2021.

Zhu, Z., Kollias, P., Yang, F., and Luke, E.: On the Estimation of In-Cloud Vertical Air Motion Using Radar Doppler Spectra, Geophys. Res. Lett., 48, e2020GL090682, https://doi.org/10.1029/2020GL090682, 2021.